Research Article Vol. 9, No. 8 | 1 Aug 2018 | BIOMEDICAL OPTICS EXPRESS 3974
Biomedical Optics EXPRESS

Quantitative two-photon microscopy imaging analysis of human skin to evaluate enhanced transdermal delivery by hybrid-type multi-lamellar nanostructure

JINHYO AHN,[1,2] KYEONG HU KIM,[3] KIBAEK CHOE,[1,2] JOO HYUCK LIM,[3] SEUNG KI LEE,[3] YEON SOOK KIM,[3] AND PILHAN KIM[1,2,4,*]

[1]*Graduate School of Nanoscience and Technology, Korea Advanced Institute of Science and Technology (KAIST), 291 Deahak-ro, Yuseong-gu, Daejeon 34141, South Korea*
[2]*KI for Health Science and Technology (KIHST), Korea Advanced Institute of Science and Technology (KAIST), 291 Deahak-ro, Yuseong-gu, Daejeon 34141, South Korea*
[3]*Biotechnology Research Institute, CELLTRION, 23 Academy-ro, Yeonsu-gu, Incheon 22014, South Korea*
[4]*Graduate School of Medical Science and Engineering, Korea Advanced Institute of Science and Technology (KAIST), 291 Deahak-ro, Yuseong-gu, Daejeon 34141, South Korea*
[*]*pilhan.kim@kaist.ac.kr*

Abstract: Transdermal skin delivery is a method to transport various topical formulations to a deeper skin layer non-invasively. Permeability analysis of many delivering agents has been mostly conducted by a simple tape stripping method. However, it cannot reveal a detailed depth-dependent distribution profile of transdermally delivered agents in the skin. In this work, we achieved a cellular-level depth-defined visualization of fluorophore-labelled human epidermal growth factor (EGF) transdermally delivered to human skin by using encapsulation with common liposomes and newly fabricated multi-lamellar nanostructures using a custom-design two-photon microscopy system. It was able to generate 3D reconstructed images displaying the distribution of human EGF inside the human skin sample with high-resolution. Based on a depthwise fluorescence intensity profile showing the permeation of human EGF, a quantitative analysis was performed to assess the transdermal delivery efficacy achieved by each formulation, showing a significant improvement of the efficacy with the utilization of multi-lamellar nanostructure.

OCIS codes: (170.2520) Fluorescence microscopy; (170.6900) Three-dimensional microscopy; (170.1870) Dermatology; (170.6930) Tissue; (120.4290) Nondestructive testing.

References and links

1. C. Herkenne, I. Alberti, A. Naik, Y. N. Kalia, F. X. Mathy, V. Préat, and R. H. Guy, "In vivo methods for the assessment of topical drug bioavailability," Pharm. Res. **25**(1), 87–103 (2008).
2. M. R. Prausnitz, S. Mitragotri, and R. Langer, "Current status and future potential of transdermal drug delivery," Nat. Rev. Drug Discov. **3**(2), 115–124 (2004).
3. M. T. Tsai, I. C. Lee, Z. F. Lee, H. L. Liu, C. C. Wang, Y. C. Choia, H. Y. Chou, and J. D. Lee, "In vivo investigation of temporal effects and drug delivery induced by transdermal microneedles with optical coherence tomography," Biomed. Opt. Express **7**(5), 1865–1876 (2016).
4. T. Blagus, B. Markelc, M. Cemazar, T. Kosjek, V. Preat, D. Miklavcic, and G. Sersa, "In vivo real-time monitoring system of electroporation mediated control of transdermal and topical drug delivery," J. Control. Release **172**(3), 862–871 (2013).
5. M. R. Prausnitz and R. Langer, "Transdermal drug delivery," Nat. Biotechnol. **26**(11), 1261–1268 (2008).
6. J. D. Bos and M. M. H. M. Meinardi, "The 500 Dalton rule for the skin penetration of chemical compounds and drugs," Exp. Dermatol. **9**(3), 165–169 (2000).
7. M. Essendoubi, C. Gobinet, R. Reynaud, J. F. Angiboust, M. Manfait, and O. Piot, "Human skin penetration of hyaluronic acid of different molecular weights as probed by Raman spectroscopy," Skin Res. Technol. **22**(1), 55–62 (2016).

#330184 https://doi.org/10.1364/BOE.9.003974
Journal © 2018 Received 26 Apr 2018; revised 15 Jun 2018; accepted 23 Jul 2018; published 31 Jul 2018

Biomedical Optics EXPRESS

8. Y. Zhu, C. S. Choe, S. Ahlberg, M. C. Meinke, U. Alexiev, J. Lademann, and M. E. Darvin, "Penetration of silver nanoparticles into porcine skin ex vivo using fluorescence lifetime imaging microscopy, Raman microscopy, and surface-enhanced Raman scattering microscopy," J. Biomed. Opt. **20**(5), 051006 (2014).
9. D. Mohammed, K. Hirata, J. Hadgraft, and M. E. Lane, "Influence of skin penetration enhancers on skin barrier function and skin protease activity," Eur. J. Pharm. Sci. **51**, 118–122 (2014).
10. D. Mahrhauser, M. Hoppel, J. Schöll, L. Binder, H. Kählig, and C. Valenta, "Simultaneous analysis of skin penetration of surfactant and active drug from fluorosurfactant-based microemulsions," Eur. J. Pharm. Biopharm. **88**(1), 34–39 (2014).
11. B. Yu, C. Y. Dong, P. T. C. So, D. Blankschtein, and R. Langer, "In vitro visualization and quantification of oleic acid induced changes in transdermal transport using two-photon fluorescence microscopy," J. Invest. Dermatol. **117**(1), 16–25 (2001).
12. T. M. Allen and P. R. Cullis, "Liposomal drug delivery systems: From concept to clinical applications," Adv. Drug Deliv. Rev. **65**(1), 36–48 (2013).
13. V. P. Torchilin, "Multifunctional, stimuli-sensitive nanoparticulate systems for drug delivery," Nat. Rev. Drug Discov. **13**(11), 813–827 (2014).
14. O. C. Farokhzad and R. Langer, "Impact of Nanotechnology on Drug Delivery," ACS Nano **3**(1), 16–20 (2009).
15. J. Batalla, H. Cabrera, E. San Martín-Martínez, D. Korte, A. Calderón, and E. Marín, "Encapsulation efficiency of CdSe/ZnS quantum dots by liposomes determined by thermal lens microscopy," Biomed. Opt. Express **6**(10), 3898–3906 (2015).
16. V. P. Torchilin, "Recent advances with liposomes as pharmaceutical carriers," Nat. Rev. Drug Discov. **4**(2), 145–160 (2005).
17. B. Dubertret, P. Skourides, D. J. Norris, V. Noireaux, A. H. Brivanlou, and A. Libchaber, "In vivo imaging of quantum dots encapsulated in phospholipid micelles," Science **298**(5599), 1759–1762 (2002).
18. T. Nii and F. Ishii, "Encapsulation efficiency of water-soluble and insoluble drugs in liposomes prepared by the microencapsulation vesicle method," Int. J. Pharm. **298**(1), 198–205 (2005).
19. M. J. Lawrence and G. D. Rees, "Microemulsion-based media as novel drug delivery systems," Adv. Drug Deliv. Rev. **45**(1), 89–121 (2000).
20. D. R. Arifin and A. F. Palmer, "Determination of size distribution and encapsulation efficiency of liposome-encapsulated hemoglobin blood substitutes using asymmetric flow field-flow fractionation coupled with multi-angle static light scattering," Biotechnol. Prog. **19**(6), 1798–1811 (2003).
21. S. Martins, B. Sarmento, D. C. Ferreira, and E. B. Souto, "Lipid-based colloidal carriers for peptide and protein delivery--liposomes versus lipid nanoparticles," Int. J. Nanomedicine **2**(4), 595–607 (2007).
22. F. Syring, H. J. Weigmann, S. Schanzer, M. C. Meinke, F. Knorr, and J. Lademann, "Investigation of Model Sunscreen Formulations Comparing the Sun Protection Factor, the Universal Sun Protection Factor and the Radical Formation Ratio," Skin Pharmacol. Physiol. **29**(1), 18–23 (2016).
23. J. Lademann, U. Jacobi, C. Surber, H. J. Weigmann, and J. W. Fluhr, "The tape stripping procedure--evaluation of some critical parameters," Eur. J. Pharm. Biopharm. **72**(2), 317–323 (2009).
24. U. Lindemann, K. Wilken, H. J. Weigmann, H. Schaefer, W. Sterry, and J. Lademann, "Quantification of the horny layer using tape stripping and microscopic techniques," J. Biomed. Opt. **8**(4), 601–607 (2003).
25. T. Y. Tseng, C. S. Yang, T. H. Tsai, Y. F. Chen, and C. Y. Dong, "Dynamic characterization of hydrophobic and hydrophilic solutes in oleic-acid enhanced transdermal delivery using two-photon fluorescence microscopy," Appl. Phys. Lett. **105**(16), 163702 (2014).
26. R. M. Hathout and M. Nasr, "Transdermal delivery of betahistine hydrochloride using microemulsions: physical characterization, biophysical assessment, confocal imaging and permeation studies," Colloids Surf. B Biointerfaces **110**, 254–260 (2013).
27. D. C. Carrer, C. Vermehren, and L. A. Bagatolli, "Pig skin structure and transdermal delivery of liposomes: a two photon microscopy study," J. Control. Release **132**(1), 12–20 (2008).
28. J. M. Andanson, K. L. A. Chan, and S. G. Kazarian, "High-Throughput Spectroscopic Imaging Applied to Permeation Through the Skin," Appl. Spectrosc. **63**(5), 512–517 (2009).
29. B. Balázs, P. Sipos, C. Danciu, S. Avram, C. Soica, C. Dehelean, G. Varju, G. Erős, M. Budai-Szűcs, S. Berkó, and E. Csányi, "ATR-FTIR and Raman spectroscopic investigation of the electroporation-mediated transdermal delivery of a nanocarrier system containing an antitumour drug," Biomed. Opt. Express **7**(1), 67–78 (2016).
30. M. Moothanchery, R. Z. Seeni, C. Xu, and M. Pramanik, "In vivo studies of transdermal nanoparticle delivery with microneedles using photoacoustic microscopy," Biomed. Opt. Express **8**(12), 5483–5492 (2017).
31. Y. Sun, J. W. Su, W. Lo, S. J. Lin, S. H. Jee, and C. Y. Dong, "Multiphoton polarization imaging of the stratum corneum and the dermis in ex-vivo human skin," Opt. Express **11**(25), 3377–3384 (2003).
32. P. Kim, M. Puoris'haag, D. Côté, C. P. Lin, and S. H. Yun, "In vivo confocal and multiphoton microendoscopy," J. Biomed. Opt. **13**(1), 010501 (2008).
33. I. Veilleux, J. A. Spencer, D. P. Biss, D. Cote, and C. P. Lin, "In vivo cell tracking with video rate multimodality laser scanning microscopy," Ieee J Sel Top Quant **14**(1), 10–18 (2008).
34. S. F. Ng, J. J. Rouse, F. D. Sanderson, V. Meidan, and G. M. Eccleston, "Validation of a Static Franz Diffusion Cell System for In Vitro Permeation Studies," AAPS PharmSciTech **11**(3), 1432–1441 (2010).
35. N. A. Belsey, N. L. Garrett, L. R. Contreras-Rojas, A. J. Pickup-Gerlaugh, G. J. Price, J. Moger, and R. H. Guy, "Evaluation of drug delivery to intact and porated skin by coherent Raman scattering and fluorescence microscopies," J. Control. Release **174**, 37–42 (2014).

Biomedical Optics EXPRESS

36. B. Godin and E. Touitou, "Transdermal skin delivery: Predictions for humans from in vivo, ex vivo and animal models," Adv. Drug Deliv. Rev. **59**(11), 1152–1161 (2007).
37. N. Alnasif, C. Zoschke, E. Fleige, R. Brodwolf, A. Boreham, E. Rühl, K. M. Eckl, H. F. Merk, H. C. Hennies, U. Alexiev, R. Haag, S. Küchler, and M. Schäfer-Korting, "Penetration of normal, damaged and diseased skin - An in vitro study on dendritic core-multishell nanotransporters," J. Control. Release **185**, 45–50 (2014).
38. W. S. Chiu, N. A. Belsey, N. L. Garrett, J. Moger, G. J. Price, M. B. Delgado-Charro, and R. H. Guy, "Drug delivery into microneedle-porated nails from nanoparticle reservoirs," J. Control. Release **220**(A), 98–106 (2015).

1. Introduction

Skin is a barrier composed of three distinguishable layers: stratum corneum, epidermis and dermis, which protects the body from undesirable substances such as virus and bacteria [1, 2]. To facilitate an effective barrier function against invading pathogens, the skin has highly organized complex network of keratinocytes, capillaries, and various immune cells through epidermis and dermis. As an alternative method to conventional oral or parenteral delivery of drug, there has been increasing interests to establish a transdermal delivery method [3–6] and develop various formulations to enhance the delivery efficacy [7–11]. However, still an efficient delivery of functional or therapeutic agents through the skin barrier has remained as a difficult challenge in the field of cosmetics and pharmaceutical industry.

Liposome which was proposed as drug delivery system is a lipid bilayer vesicle consist of amphipathic phospholipids and it resembles the structure of a cellular membrane [12–14]. It is a traditional type of nanoparticle which has been extensively investigated for pharmacological treatment and diagnostic application [15–17]. Hydrophilic substances could be encapsulated in the internal aqueous compartment of the liposome, on the other hand, hydrophobic substances could be loaded in the lipid bilayer. To establish the liposome as an effective carrier for transdermal delivery to deliver the functional agents to the targeted layer of the skin, encapsulation method to produce liposomes with high encapsulation efficiency and homogeneous size is critical [18–20]. However, encapsulating efficacy of general liposome is quite low, typically about 10~20%, because of small volume ratio of the internal aqueous compartment [20, 21]. To overcome this shortcoming, we newly fabricated a protein-lipid hybrid-type multi-lamellar nanostructured vesicle consists of a cationic lipid, 1,2-dioleoyl-3-trimethylammonium-propane (DOTAP), which can potentially be an effective carrier to deliver functional agents such as human epidermal growth factor (EGF) into the dermal layer with high physiological activity. In addition, the DOTAP hybrid-type multi-lamellar nanostructure, a 'DOTAP complex' in short, can be produced without the necessary of high pressure and temperature for a typical process to obtain the general liposome.

Currently, the most common method to analyze the permeation of agents into the skin is simple tape stripping method; the removal of a stratum corneum by tape stripping at a specific time point after the application of agents [22–24]. However it could only provide information about the concentration of agents in the removed layer of stratum corneum, thereby it could not reveal a detailed depth-dependent distribution profile of the applied agents in the skin from the epidermis to the deeper dermal layers. In the process of maximizing the delivery efficacy by adjusting multiple confounding variables such as formulation, delivery method, duration, and agent types, a non-destructive optical analysis method to quantify the permeation of various agents into the deeper skin layer is highly desirable [25–31]

In this study, as a novel effective carrier for transdermal delivery, we utilized a newly fabricated a multi-lamellar nanostructure, DOTAP complex, encapsulating human EGF with high efficacy. A custom-built laser-scanning two-photon microscopy system capable of optical sectioning imaging of the *ex vivo* human skin layer was used to establish a non-invasive quantitative analysis method to assess the efficacy of DOTAP complex for transdermal delivery of human EGF. To visualize the permeation of human EGF into the skin, a fluorescein isothiocyanate tagged EGF (FITC-EGF) was used as a model agent. Three-dimensional imaging of human skin sample applied with free-form FITC-EGF and encapsulated FITC-EGF with two types of formulations, general liposome and DOTAP

Biomedical Optics EXPRESS

complex, was performed. A quantitative analysis of three-dimensional distribution of transdermally delivered FITC-EGF in the skin layer were performed based on fluorescence signal of FITC, showing enhanced efficacy of transdermal delivery with DOTAP complex formulation.

2. Methods

2.1 Custom-built laser scanning two-photon microscopy

Using a custom-built laser scanning two-photon microscopy [32, 33], the permeation or distribution of transdermally delivered FITC-EGF in the human skin sample were fluorescently visualized. The schematic of the two-photon imaging system to visualize the depth-dependent fluorescence profiles in the skin layers is shown in Fig. 1(a). A mode-locked tunable femtosecond titanium-sapphire pulse laser (690~1020 nm, 80 MHz, Chameleon Ultra, Coherent) was used as a two-photon excitation source. A half-wave plate (10RP52-2, Newport) combined with a Glan-Laser polarizer (10GL08AR.16, Newport) were used to manually control the femtosecond laser power. The fast X-axis beam scanning at 17.28 kHz was achieved by using a rotating gold-coated polygon mirror (BMC-7, Lincoln Laser). Y-axis beam scanning at 30Hz achieved by a galvanometer-based scanning mirror (6240H, Cambridge Technology). The two-dimensional raster-scanning laser beam was delivered to a commercial water-immersion objective lens (CFI75 Apo LWD 25XW, NA 1.1, Nikon) through a dichroic beam splitter (DBS1; FF705-Di01, Semrock), providing imaging field of view of 440 μm x 440 μm. Three-color fluorescence signals were spectrally divided by two dichroic beam splitters (DBS2; FF405-Di03, DBS3; FF555-Di02, Semrock) and then simultaneously detected by photomultiplier tubes (R7518, Hamamatsu) through bandpass filters (BPF1; FF01-475/35, BPF2; FF01-525/45, BPF3; FF01-585/40, Semrock).

2.2 Preparation of general liposome and DOTAP multi-lamellar nanostructure

General liposome as shown in Fig. 1(b) was fabricated by a high pressure homogenization method. An oil phase was prepared by dissolving hydrogenated phospholipid, triglycerides, DEA-cetylphosphate in ethanol at 60°C. A water phase was prepared separately by dissolving sodium ascorbyl phosphate, EDTA and EGF tagged with FITC (cat no. F7250, Sigma-Aldrich). The water and oil phases were quickly mixed with a homo-mixer and passed 3 times through a high pressure homogenizer (MN200-15P, Micronox, Korea) at 1000 bar (15,000 psi).

The cationic lipid DOTAP (1,2-dioleoyl-3-trimethylammonium-propane, Lipoid Inc.) was dissolved in 1 ml of ethanol and mixed in a round glass flask. In a rotary evaporator, nitrogen was flushed into the lipid solution at low rate to remove the ethanol. Thereby a thin lipid layer was formed when the lipid was dried. The lipid layer was dried further in a vacuum for 12 hours to completely remove the remaining ethanol. 1 ml of purified water was added to the prepared lipid layer by stirring at 37°C for 2 hours, to obtain the cationic empty uni-lamellar liposomes composed of DOTAP, extruded several times through a polycarbonate membrane (Avanti Polar Lipid Inc.) having a uniform pore size in a diameter of 100 nm. A solution containing the empty DOTAP uni-lamellar liposomes and FITC tagged EGF were mixed with purified water at normal temperature to obtain the DOTAP hybrid-type multi-lamellar nanostructures as shown in cryogenic transmission electron microscopic image (JEM-3011, JEOL Ltd.) of Fig. 1(b).

2.3 Human skin preparation and two-photon imaging analysis

Human skin samples were obtained through ZenBio, Inc. (Morrisville, NC, USA), which were collected from the abdomen of normal healthy Caucasian donors in conformance with FDA regulations and guidelines. Using a micropipette, 250 ppm (200 μl) of FITC-EGF encapsulated with general liposome or DOTAP multi-lamellar nanostructure was applied to

Biomedical Optics EXPRESS

the human skin which cut to 2 × 2 cm width and placed in the Franz diffusion cell system [34]. Phosphate-buffered saline (pH 7.4, 5 ml) was filled in the receptor of the chamber and maintained at 33.5 degrees. Also skin samples applied with free-form FITC-EGF were prepared as a baseline control group. To investigate time-dependent skin permeation of FITC-EGF, each sample was placed in the Franz diffusion cell system for 12 and 24 hours respectively as shown in Fig. 1(b). All skin samples were mounted between coverslips and slide glasses for two-photon imaging analysis. The laser wavelength for two-photon excitation was 840 nm and the laser power delivered to the skin sample was 90 mW. Sequential z-stack images were captured at 3 μm depth intervals from the skin surface until the fluorescence signal became undetectable. From the z-tack images acquired in three randomly selected spots, the average intensity of pixels in the areas with the size of 25,000 ~40,000 μm^2 those were carefully delineated to be devoid of ripples and hair follicles was calculated using 'plot z-axis profile' plugins in ImageJ (NIH, USA) to plot intensity profiles of FITC signal versus the depth in the skin [35]. Skin areas involved with overly bright pixels were avoided since the strong signals could affected the numerical results leading to inaccurate analysis. In addition, to remove the uncertainty in analyzing the permeation of FITC-EGF from the non-flat skin surface, the '0 μm' depth in each analyzed area was individually identified as the position when the observed FITC signal intensity at each area became maximum during the sequential z-stack imaging. XZ-axis orthogonal view of the skin was reconstructed using 'volume viewer' plugins in ImageJ. Figure 1(c) shows representative cellular-level microscopic images obtained from the surface of the human skin at 24 hours after the application of free-form FITC-EGF and encapsulated FITC-EGF with general liposome and DOTAP complex, which clearly shows the outline of corneocyte permeated with the FITC-EGF.

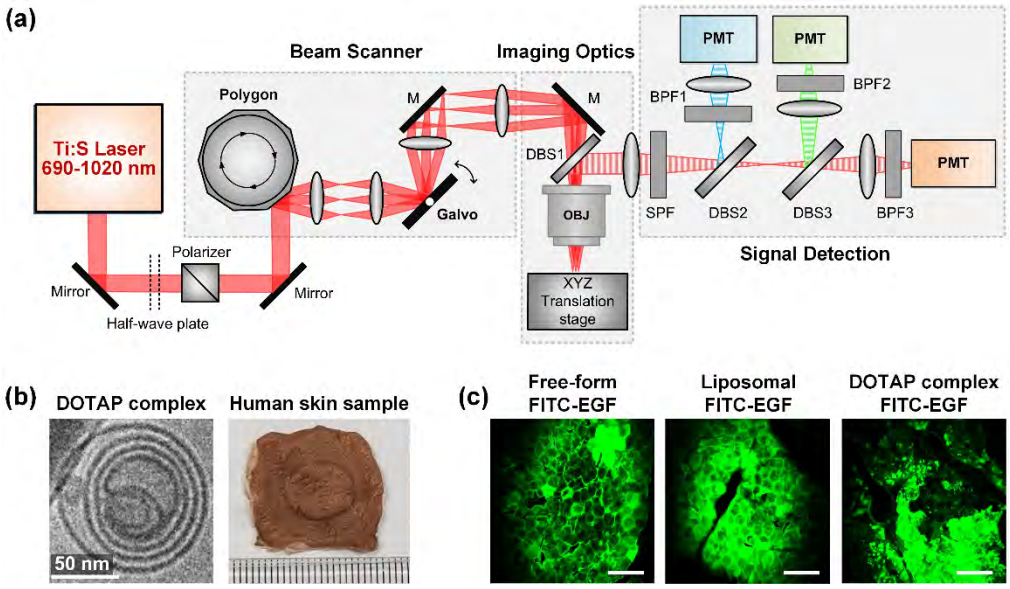

Fig. 1. (a) Schematic of a custom-built laser-scanning two-photon microscopy for imaging of human skin sample. M, mirror; OBJ, Objective lens; SPF, single band pass filter; DBS, dichroic beam splitter; BPF, band pass filter; PMT, photomultiplier tube. (b) Cryogenic electron microscopic image of DOTAP hybrid-type multi-lamellar nanostructure; DOTAP complex (left), and the photograph of human skin sample (right) prepared using a Franz cell diffusion system. (c) Representative images acquired from human skin samples after the application of free-form FITC-EGF and encapsulated FITC-EGF with general liposome and DOTAP complex. Scale bars: 100 μm.

Biomedical Optics EXPRESS

3. Result

In previous studies [36–38], experiments have been conducted to determine a time-dependent changes in permeation of fluorophores or functional materials applied to the skin surface. To compare the changes in permeation depth of different formulated FITC-EGF over time after the application, the human skins applied with free-form, liposomal and DOTAP complex FITC-EGF were placed in the Franz diffusion cell system for 12 or 24 hours. Figure 2 and Fig. 3 show the sequential z-stack images and quantitate analysis of FITC-EGF permeation into the inner layer of human skin sample after 12 hours and 24 hours, respectively.

Figure 2(a) shows representative sequential z-stack images of human skin samples obtained with 3 μm depth interval at 12 hours after the application of free-form and encapsulated FITC-EGF. As shown in Fig. 2(b), depth-dependent distribution of FITC-EGF permeated into the skin could be visualized in XZ orthogonal view or 3D volumetric images, which were reconstructed using the sequential z-stack images. Figure 2(c-d) shows a normalized FITC-EGF signal intensity along the z-axis from surface to dermal layer of the human skin samples. In each experimental group, average fluorescence intensity was measured in randomly defined 3 spots from 8 different human skin samples. Average intensity of FITC-EGF measured from the skin applied with DOTAP complex encapsulated FITC-EGF was higher than those measured in other samples up to approximately 40 μm depth as shown in Fig. 2(d), suggesting enhanced delivery of FITC-EGF. Figure 2(e) shows the measured penetration depth of FITC-EGF with different thresholds of 50, 20, 10, and 5% of fluorescence intensity at the skin surface. Penetration depth of FITC-EGF encapsulated with DOTAP complex was greater than FITC-EGF encapsulated with general liposome with 5% threshold (Liposomal FITC: 23.2 ± 12.3 μm, DOTAP complex FITC: 29.9 ± 10.5 μm), whereas no statistically significant difference was observed with 10% threshold. Interestingly, penetration depth of free-form FITC-EGF was greater than that of general-liposome encapsulated FITC-EGF and slightly smaller than DOTAP complex encapsulated FITC-EGF with no statistical significance.

Biomedical Optics EXPRESS

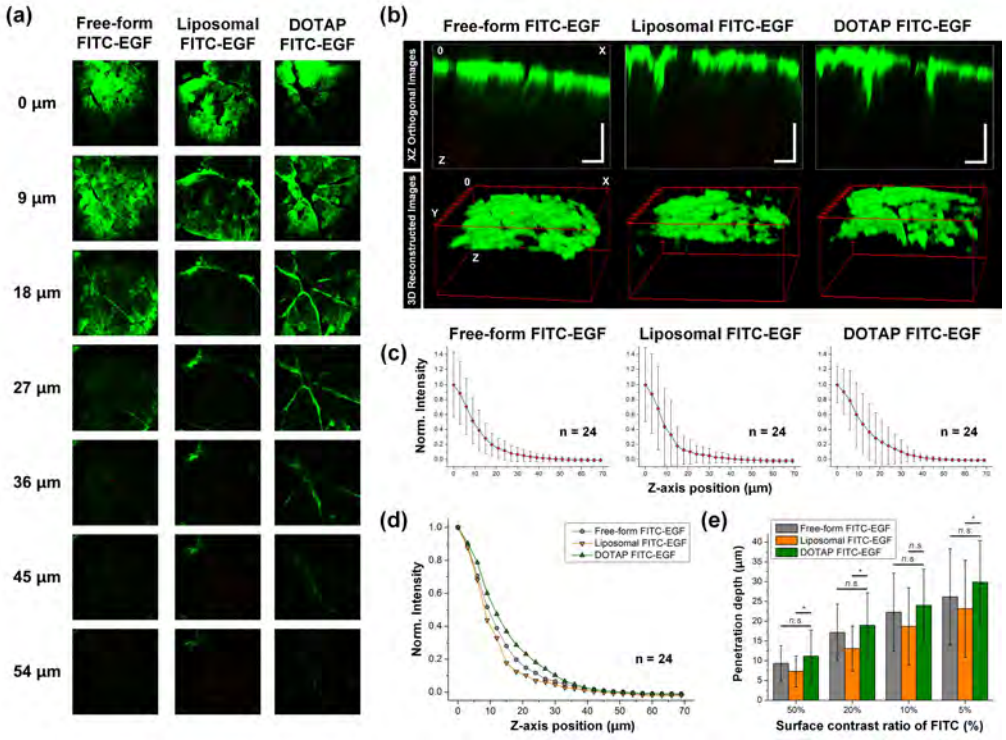

Fig. 2. (a) Representative sequential images of human skin samples at 12 hours after the application of free-form FITC-EGF, encapsulated FITC-EGF with general liposome or DOTAP complex. (b) Reconstructed images in XZ orthogonal view and 3D view. Scale bars: 50 μm. (c-d) Averaged normalized FITC-EGF signal intensity along the z-axis from surface to dermal layer of the human skin samples. (e) Penetration depth of FITC-EGF with different thresholds of 50, 20, 10, and 5% of fluorescence intensity measured at the skin surface.

We performed similar analysis with the human skins at 24 hours application of free-form, liposomal and DOTAP complex FITC-EGF in the Franz diffusion cell system. Figure 3(a) shows representative sequential z-stack images. Figure 3(b) shows distribution of FITC-EGF in XZ orthogonal view or 3D volumetric images. Figure 3(c-d) shows a normalized FITC-EGF signal intensity from surface to dermal layer of the human skin samples. In each experimental group, average fluorescence intensity was measured in randomly defined 3 spots from 3 different human skin samples. Up to approximately 60 μm depth into the human skin sample, average intensity of FITC-EGF with DOTAP complex encapsulated FITC-EGF was higher than those with other groups. Figure 3(e) shows the measured penetration depth of FITC-EGF with different thresholds of 50, 20, 10, and 5% of fluorescence intensity at the skin surface. Similar to the measurement result at 12 hours application with 5% threshold, the penetration depth of FITC-EGF encapsulated with DOTAP complex was much greater than FITC-EGF encapsulated with general liposome (Liposomal FITC: 26.9 ± 7.6 μm, DOTAP complex FITC: 48.1 ± 5.4 μm). Notably, not only with 5% threshold but also with 10% threshold, there was statistically significant enhancement in penetration depth with DOTAP complex encapsulation (Liposomal FITC: 20.3 ± 5.8 μm, DOTAP complex FITC: 35.5 ± 4.6 μm), which was not statistically significant at 12 hours application as shown in Fig. 3(e).

Biomedical Optics EXPRESS

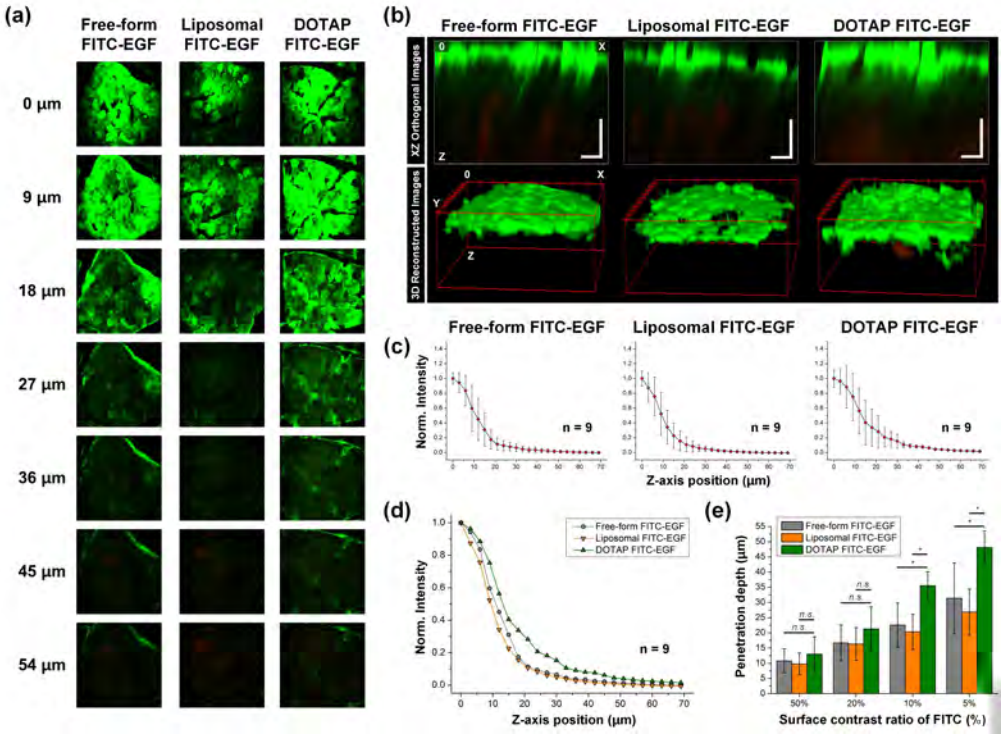

Fig. 3. (a) Representative sequential images of human skin samples at 24 hours after the application of free-form FITC-EGF, encapsulated FITC-EGF with general liposome or DOTAP complex. (b) Reconstructed images in XZ orthogonal view and 3D view. Scale bars: 50 μm. (c-d) Averaged normalized FITC-EGF signal intensity along the z-axis from surface to dermal layer of the human skin samples. (e) Penetration depth of FITC-EGF with different thresholds of 50, 20, 10, and 5% of fluorescence intensity measured at the skin surface.

Intensity profiles of the FITC-EGF signal in Fig. 2(c, d) and Fig. 3(c, d) showed a rapid decay at the epidermal layer from the maximum of the skin surface. Relatively large standard deviations in the epidermal layer were mostly attributed to inhomogeneity of the *ex-vivo* human skin samples those were affected by various factors causing differences between the skin samples. Despite the similar sharp decline showed in all three groups, the fluorescence intensity of FITC-EGF encapsulated with DOTAP complex was much higher in the inner layer of skin. These results strongly suggest a high encapsulation ability of the DOTAP complex could contribute the improved delivery of the FITC-EGF into the deeper skin.

4. Conclusion

We demonstrated a quantitative analysis based on sequential z-stack images was conducted to compare the skin permeability of FITC-EGF encapsulated with newly fabricated formulation, DOTAP complex, and conventional general liposome. We utilized a custom-design two-photon microscopy technique for the depth-defined visualization of fluorescently tagged agent, FITC-EGF, in the *ex vivo* human skin layer for quantitative analysis of transdermal delivery efficacy. Significantly enhanced delivery of FITC-EGF into the human skin with the encapsulation by DOTAP complex was clearly visualized. This method can be widely utilized to assess the transdermal delivery efficacy in the process of optimizing a novel formulation or developing an efficient method to deliver various functional agent into the deep skin layer with a minimal disturbance in skin-barrier integrity.

Biomedical Optics EXPRESS

Funding

CELLTRION Corporation; Global Frontier Project (NRF-2013M3A6A4044716) and Basic Research Program (NRF-2017R1E1A1A01074190) funded by the Ministry of Science and ICT, Republic of Korea.

Acknowledgments

The authors would like to thank Eunjoo Song, Yoonha Hwang, Howon Seo, Soyeon Ahn, Jieun Moon, Eunji Kong, Jingu Lee, Ryul Kim, Sujung Hong for advice and helpful discussion, Soo Yun Lee and Haeun Kim for their technical assistance.

Disclosures

Jinhyo Ahn, Kibaek Choe, Pilhan Kim: CELLTRION Corporation (F) Kyeong Hu Kim, Joo Hyuck Lim, Seung Ki Lee, Yeon Sook Kim: CELLTRION Corporation (E,P,R)